Energy LAB

RESEARCH ARTICLE

Energy Lab 2023, 1, 220014

Molecular extension engineering constructing long-chain organic elastomeric interphase towards stable potassium storage

Jun Peng[1,§], Xianhui Yi[1,§], Ling Fan[1], Jiang Zhou[2*] and Bingan Lu[1,3*]

Electrolytes are critical for achieving high performance potassium ion batteries (PIBs) because of their ability to modulate the solid electrolyte interphase (SEI). However, the compositions of SEI in conventional electrolytes are either anion-derived inorganic-rich compounds or solvent molecule-derived short-chain organic-rich compounds. These SEI are generally inelastic and cannot effectively relieve the stress changes caused by volume changes during the charge/discharge processes. Here, we constructed long-chain organic-rich SEI (LO-SEI) with high elasticity by introducing a green and harmless long-chain solvent of dicaprylyl carbonate (DCC), thus greatly improving the performance of PIBs. As a result, a long stability of more than 1500 cycles (86.7% capacity retention) for graphite half-cells and more than 3700 hours for K||K symmetric cells are achieved. In addition, the elastomeric LO-SEI-based full cell is capable of stable operating for more than 130 cycles (84.3% capacity retention). This work may open new ideas for constructing long-chain elastic interphases to achieve high-performance batteries.

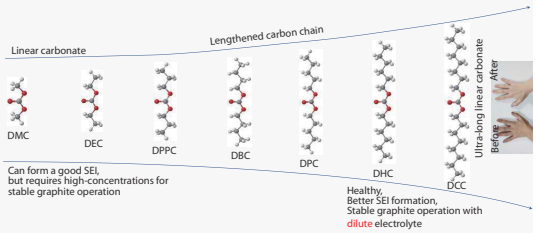

Potassium-ion batteries (PIBs) are one of the most promising energy storage devices, taking advantage of the abundant potassium resources and the low standard reduction potential of potassium[1–4]. As known, the graphite anode possesses the advantages of low cost and high energy density, and is used as the most common electrode material in the field of secondary batteries[5]. However, the cycling stability of graphite anodes is limited in conventional electrolytes. Therefore, the development of new electrolytes capable of stabilizing graphite anodes is essential to facilitate the industrialization of PIBs.

The electrolyte engineering, including the development of new salts[6,7] or new solvents[8] or changes in salt concentration[9], have significant impact on the electrochemical performance of battery. Particularly, the decomposition of electrolyte could construct solid electrolyte interphase (SEI) on the graphite anode, which is a promising pathway for regulate battery performance[10–16]. Broadly speaking, the currently conventional electrolyte-generated SEI is mainly divided into anion-derived inorganic-rich SEI (I-SEI)[17,18] or solvent molecule-derived short-chain organic-rich SEI[19,20] (SO-SEI). Fervent researches had proved the I-SEI can effectively facilitate ion transport[21–28], while it is also fragile. The imperfection of I-SEI come up with repeatedly fracture and growth due to the volume change during the cycling[29–32], subsequently with electrolyte sacrifice[33]. Moreover, the anion-dominated behavior of I-SEI generally requires a relatively high salt concentration (> 3 M), while the high cost and viscosity have hindered their practical application [in this work, "M" stands for molar concentration, i.e., mole of salt dissolved in a liter of solvent (not the electrolyte solution)][34–37]. Current solvent molecule-derived SO-SEI possesses the merits of low Young's modulus, better flexibility and non-fragility[29,38–40]. However, SO-SEI has a very short life span and cannot be popularized on a large scale[38,41,42]. In addition, many electrolyte solvents are toxic and may cause damage to the human body when the leakage of electrolyte was happened. Therefore, exploring green solvents with improved elasticity of SEI to relieve the volume changes might be more feasible to stabilize PIBs.

Due to the failure of SO-SEI, we started to consider the use of long-chain solvents to modulate the organic interphase. Herein, we expanded the short molecular chain of the commercial electrolyte dimethyl carbonate (DMC) to obtain the green and harmless long-chain solvent, dicaprylyl carbonate (DCC) (Figure 1a). We applied dcc solvent to our hands to confirm its biosafety. DCC is a biosafety solvent and has been commonly used as an additive in skin care products because

[1] *School of Physics and Electronics, Hunan University, Changsha 410082, China*

[2] *School of Materials Science and Engineering, Central South University, Changsha 410083, China*

[3] *State Key Laboratory of Advanced Design and Manufacturing for Vehicle Body, Hunan University, Changsha 410082, China*

* Corresponding author, E-mail: zhou_jiang@csu.edu.cn; luba2012@hnu.edu.cn

Received 4 November 2022; Accepted 10 March 2023; Published online

§These authors contributed equally to this work

DOI: 10.54227/elab.20220014

of its extremely dry skin feel and good spreading properties, comparable to volatile silicone oil. 1 M potassium bis(fluorosulfonyl)imide (KFSI) salt was dissolved in a mixture of ethylene carbonate (EC) and DCC solvents to modulate the solvation properties and organic interphase with long-chain molecules. Consequently, the graphite anode delivers more than 1500 cycles at a current density of 100 mA g^{-1} (capacity retention of 86.7%) with an average Coulombic efficiency of over 99%. Moreover, the cycle time of K||K symmetric cell exceeds 3700 hours. Compared with conventional electrolyte of 1 M KFSI in EC/diethyl carbonate (DEC), the long-chain electrolyte of 1 M KFSI-EC/DCC demonstrates superior performance.

Materials and Methods

Materials and Chemicals

KFSI (98%), DEC (99%), DCC (98%), EC (99%), polyvinylidene fluoride (PVDF), lithium bis(fluorosulfonyl)imide (LiFSI, 98%), Ketjen black, 3,4,9,10-perylenetetracarboxylic diimide (PTCDI, 95%) were purchased from Shanghai Macklin (China) Biochemical Co., Ltd. Aluminum foil, copper foil and commercial graphite were purchased from Kejing (China) Materials Technology Co., Ltd. All materials were used as received.

Electrolyte and Electrode Preparation

The graphite anode was prepared by mixing the active material with Ketjen black and PVDF in the mass ratio of 8:1:1. Then the slurry was evenly applied to the copper foil and put into a vacuum drying oven at 80 °C for 12 hours. The loading mass of the graphite anode was approximately 0.8 mg cm^{-2}. PTCDI cathodes were prepared by mixing PTCDI powder with Ketjen black and PVDF in the mass ratio of 7:2:1. The slurry is evenly applied to the copper foil and vacuum drying at 80 °C for 24 h. The loading area of the PTCDI cathode was approximately 1 mg cm^{-2}. The electrolytes were prepared by adding different amounts of KFSI powders to the corresponding EC/DCC (1:1 in *vol.*) or EC/DEC (1:1 in *vol.*) solvent mixture, respectively, in an argon-filled glove box with oxygen and water content of < 0.1 ppm.

Electrochemical Measurements

For half-cells, graphite anodes were used as working electrodes and potassium foils as reference electrodes to prepare 2032-type coin cells with electrolytes. Glass fibers (Whatman) were adopted as the separators. The amount of electrolyte for each coin cell was approximately 80 μl. The electrochemical properties were tested using a Neware BTS-53 instrument. For full cells, graphite anodes are pre-cycled 5 times in EC/DCC and PTCDI cathodes are pre-cycled 10 times in EC/DCC electrolyte. The capacity of the anode was higher than that of the cathode (with a ratio of 1.05/1).

Material Characterizations

To characterize the X-ray photoelectron spectrometer (XPS), atomic force microscope (AFM) and transmission electron microscopy (TEM) properties of the circulating electrode, the PIBs were disassembled in a glove box and washed with EC/DCC solvents to remove the potassium salt. TEM imagines were collected using the Tecnai F20. The stress curve of SEI was measured by AFM (Bruker Dimension Icon). XPS measurements were performed using Thermo Scientific KAlpha. The electrochemical workstation tests the electrochemical impedance spectroscopy of K||graphite half-cells in the frequency range of 10^{-2}-10^{5} with a voltage amplitude of 10 mV. The thermal weight tests were carried out in the thermal gravimetric analyzer (TGA, METTLER TOLEDO TGASDTA851e).

Calculation Method

The first-principles calculations were performed in the Gaussian (G09) procedure, and the parameter mixing method uses the Lee-Yang-Parr correlation generalization function (B3LYP) The basis was set to 6-311G++G(d, p). Solvation effects was considered with an integral equation formalism variant polarization continuum (IEFPCM) model. The binding energy (E_b) between the solvent and the lithium ion was defined as defined as following:

$$E_b = E_{total} - E_K - E_{solvent} \quad (1)$$

E_{total}, E_K, and $E_{solvent}$ are the total energy of the K^+–solvent complex, K ion, and a solvent, respectively.

Result and Discussion

Because of the cost is a main factor that must be considered before doing experiments. We firstly investigated the price from the products of DMC carbon chain lengthening, and found that dipropyl carbonate (DPPC), dibutyl carbonate (DBC), dipentyl carbonate (DPC), and dihexyl carbonate (DHC) are too expensive, while DCC is very suitable (Supplementary Figure 1). In addition, the SO-SEI formed by the conventional solvation structure of the electrode solution is always inhomogeneous, which can lead to an inferior cycle life of the battery. This work uses DCC solvent to modulate the solvation structure and the organic-rich interphase, aiming to form a uniform and elastic long-chain organic-rich SEI (LO-SEI), which expected to stabilize the battery cycle and extend the operating life of the battery (Figure 1b, c). Before starting the formal experiments, we have investigated the highest occupied molecular orbital (HOMO) and lowest unoccupied molecular orbital (LUMO) energy levels as well as the physical and chemical properties of several solvents (Supplementary Tables 1, 2). DCC exhibits lower LUMO levels compared to EC and DEC, so it is preferentially reduced to form SEI on graphite anodes[43], which facilitates the acquisition of DCC-derived LO-SEI. As shown in Figure 1d, the high degree of overlap between the approach and retract curves obtained with the AFM probe force curve represents the good elasticity of SEI in the presence of LO-SEI (see detailed discussion later), especially the point 1 and 2 overlap is particularly important.

The evolution of the K metal is shown in Figure 2a. We prepared 1 M, 3 M KFSI in EC/DEC conventional electrolytes and 1 M, 2 M, 3 M KFSI in EC/DCC novel electrolytes. The K||K symmetric cells can operate for 580 hours with 1 M KFSI in EC/DEC electrolyte, which is much lower than that with 1 M KFSI in EC/DCC electrolyte (3700 hours). Moreover, the polarization voltage of K||K cells with 1 M KFSI in EC/DCC electrolyte is much lower than that with 1 M KFSI in EC/DEC electrolyte (Figure 2b), which indicates the outstanding performance of LO-SEI on stabilizing potassium-metal symmetric cells.

With 1 M KFSI in EC/DCC as electrolyte, the graphite||K cell delivers a stable cycling performance for more than 1500 cycles, maintains a reversible capacity of about 260 mAh g^{-1}

DOI: 10.54227/elab.20220014

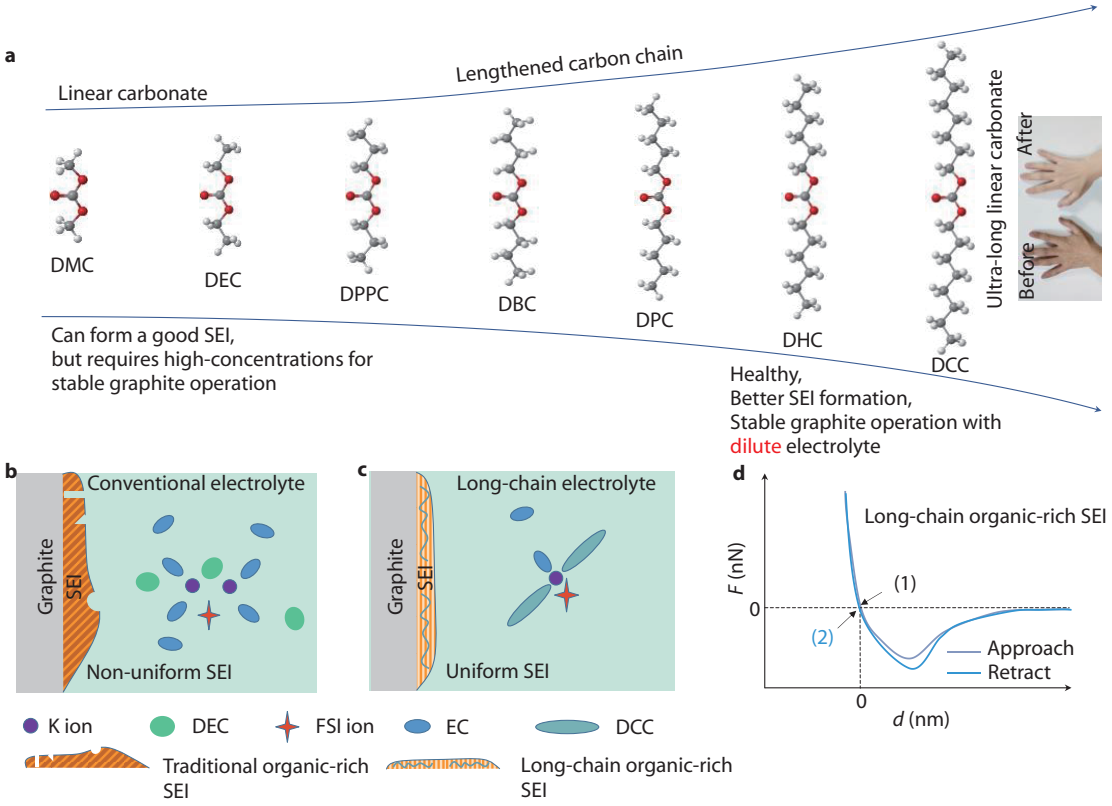

Fig. 1 **a** Molecular design to grow a range of products with terminal substituents and to regulate the solvation properties of solvent molecules. The small picture shows the comparison before and after applying the hand with DCC solvent. SEI morphology on graphite anode and solvation structure of **b** conventional and **c** long-chain electrolytes. **d** Schematic diagram of the effect of long-chain organic molecules on the elasticity of SEI.

with an average Coulombic efficiency over 99%, which could be further verified by the highly consistent charge-discharge curve after 300 cycles (Figure 2c). In contrast, the graphite||K cells using conventional low-concentration carbonate electrolytes show rapid capacity decay, and merely remain a reversible capacity of 110 mAh g^{-1} after 30 cycles (Figure 2d). Even using a high concentrated conventional electrolyte, the graphite half-cell still suffered from capacity decay, leaving a reversible capacity of only 180 mAh g^{-1} after 280 cycles.

Cycling performance, capacity retention and electrolyte concentration are the key electrochemical parameters of the cell. Figure 2e, f show some of the electrochemical properties of the commonly used electrolytes[2]. We verified the performance of the conventional concentration new long-chain electrolyte in graphite half-cells (Figure 2f), and the typical charge-discharge curves are shown in Supplementary Figure 2. It can be seen that the cycling performance of I-SEI formed with DCC electrolyte is also very good for high concentration, with 3M KFSI in EC/DCC cycling over 600 cycles (94.9% capacity retention). However, the LO-SEI with 1M KFSI in EC/DCC has a definite advantage, which is a great improvement for the PIBs. The cell has been cycled for more than 12 months, and such excellent cycling performance is a direct proof of the advantages of LO-SEI.

To verify our conjecture of LO-SEI, we performed characterization of the graphite surface after 5 cycles under several different electrolytes (Figure 3a-d). The XPS characterization results showed that all the graphite after cycling had 7 peaks corresponding to F 1*s*, O 1*s*, N 1*s*, K 2*p*, C 1*s*, S 2*s*, and S 2*p*, and it is noteworthy that the new long-chain solvent as the electrolyte in the graphite electrode sheet, a chain carbon peak can be observed around 288.9 eV[44] (Figure 3b), this could be a credential for the involvement of DCC molecules in SEI. In addition, they all have peaks such as K 2*p*, C-O (285.6 eV), C=C/C-C (284.8 eV), and several peaks have approximately the same content[45–47]. On the characteristic peaks of S 2*p* several electrolytes existed peaks of $KHSO_4$ (169.6 eV), K_2SO_4 (168.5 eV), K_2SO_3 (166.2 eV) (Figure 3c), these compounds were formed due to the decomposition of KFSI[5,48]. The difference is that the characteristic peak of $K_2S_2O_3$ (161.8 eV) is also present in both high concentration electrolytes, and the relative content of each element can be obtained by combining the results of the N 1*s* and F 1*s* tests (Supplementary Figure 3). Moreover, the results show that the organic content (ratio of C 1*s* and O 1*s*) of the 1 M EC/DCC electrolyte (64.3%) is much higher than that of the 3 M EC/DCC (58.1%) and 3M EC/DEC (49.6%) (Supplementary Figure 4), suggesting that an organic dominated SEI was formed.

In addition, we performed AFM stress tests on graphite SEI after 10 cycles with 3 M KFSI in EC/DCC, 1 M KFSI in EC/DEC, and 1 M KFSI in EC/DCC electrolytes (Figure 3e-g). Approach and retract curves represent stress curves of the probe on approach and retract. From point 1 to point 2, the AFM probe approaches the sample surface driven by the extension of the

DOI: 10.54227/elab.20220014

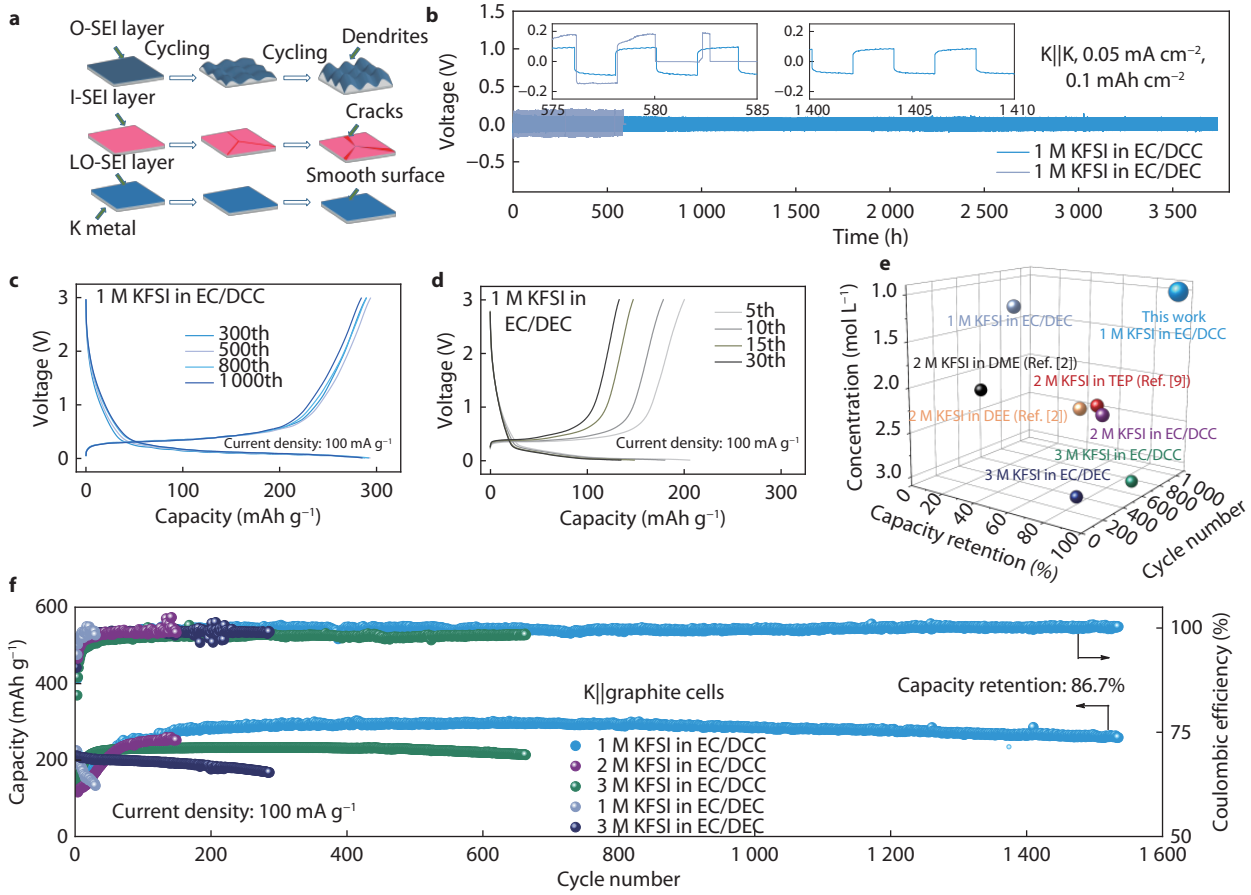

Fig. 2 **a** The schematic diagram of three kinds of SEI for K metal anode. **b** Comparison of the performance of 1 M KFSI in EC/DEC and 1 M KFSI in EC/DCC electrolytes for symmetric K||K cells at a current density of 0.05 mA cm^{-2}. Charge/discharge voltage profile of graphite anode in **c** 1 M KFSI in EC/DCC and **d** 1 M KFSI in EC/DEC electrolytes. **e** Comparison of cycling performance, concentration and capacity retention between graphite electrodes with different electrolytes cycles (TEP is triethyl phosphate, DME means 1,2-dimethoxyethane and DEE stands for 1,2-diethoxyethane). **f** Cycling performance of K||graphite cells with Coulombic efficiency with five different electrolytes at a current density of 100 mA g^{-1}.

piezoelectric body. The negative peak force between point 1 and point 2 is due to the attractive force (Van der Waals force) between the sample surface and the AFM probe[49]. The sample starts to deform at point 2 and continues to deform under the downward force exerted by the bending stress (point 2 to point 3). Point 3 to point 4 and then to point 1 represent the curve of probe retraction. For anaphylactic molecules, the SEI breaks just as the probe begins to deform and the subsequent curve is the stress on the graphite surface (Figure 3e). For organic small molecules, the approach and retract curves barely overlap indicating poor elasticity (Figure 3f). In contrast, LO-SEI has a high degree of overlap between point 2 to point 3 and point 3 to point 4 (Figure 3g), proving its good elasticity. Its poor overlap in one section may be due to the fact that in indentation tests, perturbations such as surface roughness, surface contaminants, small particle agglomeration or sliding are usually manifested as irreversible processes, which are reflected as irregular perturbations in the mechanical curves.

To observe the morphology of SEI more visually, we performed TEM characterization of graphite electrode after 10 cycles with four different electrolytes (Figure 3h, i and Supplementary Figure 5). The results show that the SEI on graphite surface is uniform and thin with the 1 M KFSI in EC/DCC electrolyte. Moreover, it can be seen that the thickness and uniformity of LO-SEI are well maintained after 50 cycles (Supplementary Figure 6), which is the direct reason why the new long-chain electrolyte can stabilize the graphite cycle.

In order to compare the thermal volatility of the two electrolytes, thermo-gravimetric tests were performed. The results of the *thermo-gravimetric analysis* (TGA) show that the weight of the EC/DEC electrolyte decreases started from 50 °C, and more than 78% of the weight decreases due to solvent volatilization after heating to 250 °C (Supplementary Figure 7). In contrast, EC/DCC electrolyte are less volatile below 250 °C, whose weight decrease of 38.34%. This indicates that EC/DCC electrolyte have a higher thermal tolerance and exhibit better thermal volatility compared to EC/DEC.

In addition, the electrochemical behaviors of DCC-based electrolytes in Li-ion batteries (LIBs) are further investigated, as shown in Supplementary Figure 8. The cycling performance of Li||graphite half-cell with 1 M LiFSI in EC/DCC electrolyte is evaluated at a current density of 100 mA g^{-1}. It can be seen that the charge-discharge curves remain highly consistent within 80 cycles (Supplementary Figure 8a), and the Coulombic efficiency is close to 100% (Supplementary Figure 8b).

DOI: 10.54227/elab.20220014

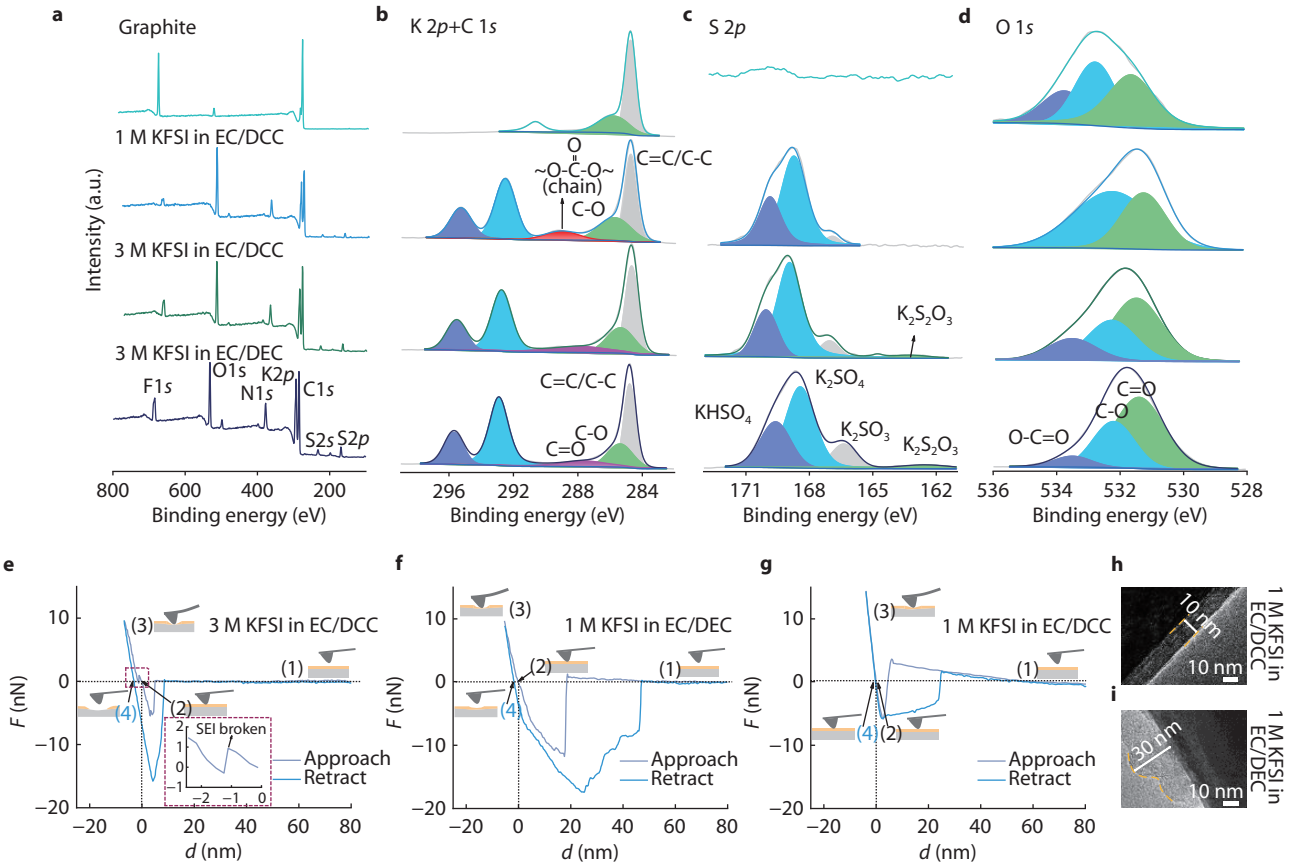

Fig. 3 XPS analysis of graphite electrode after 5 cycles with initial graphite and three kinds of electrolytes (1 M KFSI in EC/DCC, 1 M KFSI in EC/DEC, 3 M KFSI in EC/DEC). **a** Full survey XPS. **b** K 2*p* + C 1*s* XPS. **c** S 2*p* XPS. **d** O 1*s* XPS. Characterizations of the SEI formed on graphite electrodes with two different electrolytes after 20 cycles. Graphite after 10 cycles for AFM stress test of **e** 3 M KFSI in EC/DCC, **f** 1 M KFSI in EC/DEC and **g** 1 M KFSI in EC/DCC. TEM images of graphite cathodes after 10 cycles in **h** 1 M KFSI in EC/DCC and i 1 M KFSI in EC/DEC electrolytes. The yellow dashed lines indicate partial SEI.

The LO-SEI generated from DCC solvents was demonstrated to have excellent performance in the field of LIBs as well.

The binding energy has an important effect on the SEI composition[50,51]. We calculated the binding energy of the selected solvents with K ions using the first-principle calculations. The results in Supplementary Figure 9 show that DCC has the smallest interaction with K ions with a binding energy of -0.30 eV, which favors the desolvation process and the formation of LO-SEI on anode by selective decomposition[50]. We infer from the characterization (Figure 3a-g) and computational simulation results (Supplementary Figure 9) that DCC is preferentially involved in the formation of SEI.

To further verify the practicality of the long-chain solvent, we constructed a full cell with graphite as the anode and PTCDI as the cathode. We first investigated the PTCDI||K half-cell (Figure 4a, b), and found that the DCC-based electrolyte was able to increase the cycle life of PTCDI organic cathode up to 1000 cycles. Figure 4c shows the normalized charge/discharge curves of PTCDI||graphite full-cell and the PTCDI||K cathodes and graphite||K half cells. The N/P of graphite and PTCDI is about 1.1:1. Figure 4d shows the charge/discharge curves of the full-cell from 5 to 90 cycles, the good overlap of charge/discharge curves further indicating the good cycling stability of the full-cell. It can be seen that the full- cell provides a reversible capacity of 94.3 mAh g^{-1} after 130 cycles, corresponding to a capacity retention of 84.3% (Figure 4e). Figure 4f shows a comparison of the performance of 1 M KFSI in EC/DCC and conventional 1 M KFSI in EC/DEC electrolytes. By introducing DCC solvent to construct long-chain SEI, the 1 M KFSI in EC/DCC electrolyte can overcome the disadvantages of conventional 1 M KFSI in EC/DEC electrolyte, thus leading to an enhancement on cycling stability and thermal volatility.

Conclusion

In this work, a new green and harmless long-chain solvent of DCC is proposed to achieve stable operation of PIBs at low electrolyte concentrations. The DCC solvent could regulate the solvation sheath of electrolyte, leading to DCC-derived LO-SEI. The formed LO-SEI is homogeneous and highly elastic, and could further inhibit the solvent decomposition, improve the electrochemical performance of K metal and graphite anode as well as full-cells. Furthermore, this is the first application of DCC in systems involving battery electrolytes, and its excellent electrochemical performance is expected to be extended to various battery systems (Supplementary Figure 7), especially those with commercially available positive and negative electrodes (e.g., LIBs and Na-ion batteries).

DOI: 10.54227/elab.20220014

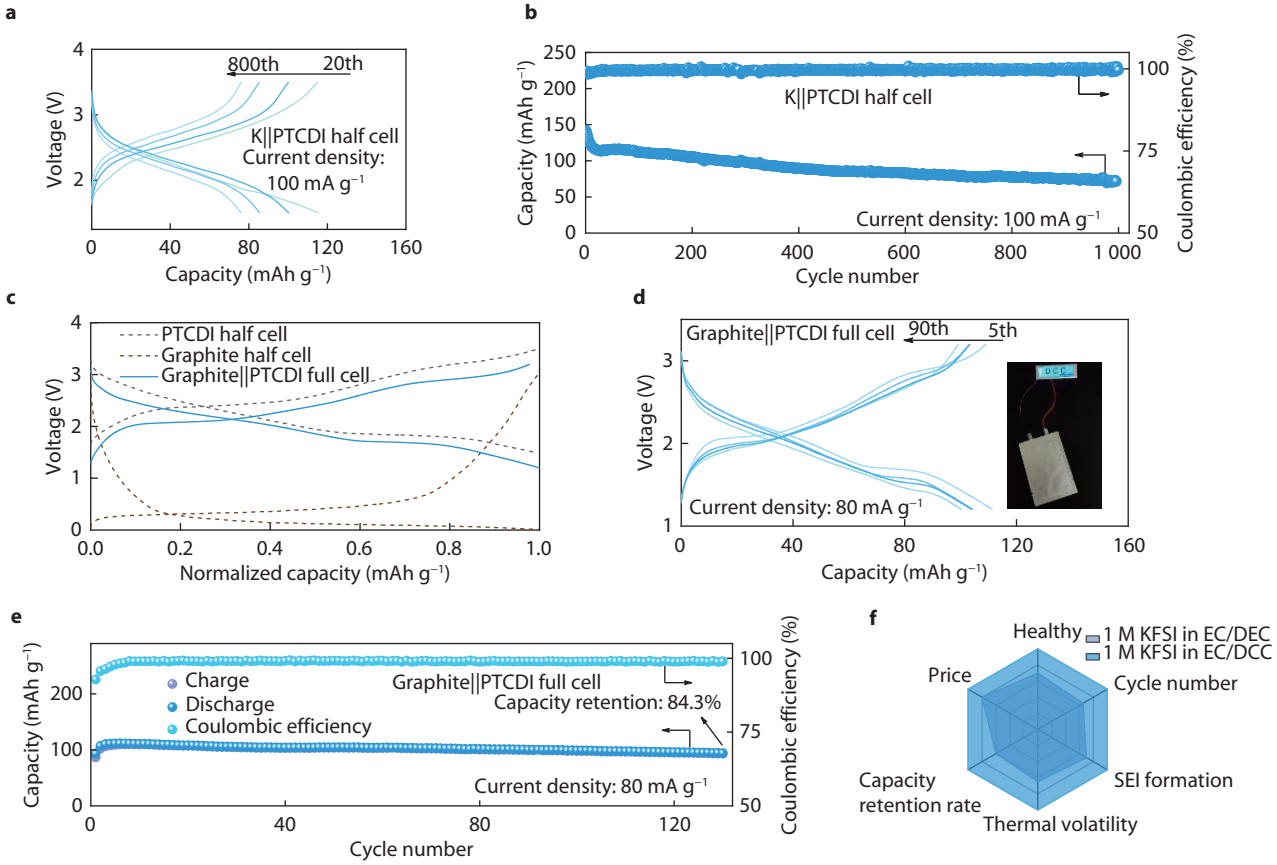

Fig. 4 **a** Charge/discharge voltage profile of PTCDI cathode in 1 M KFSI in EC/DCC electrolyte. **b** Cycling performance of K||PTCDI cell at a current density of 100 mA g^{-1}. **c** Normalized charge/discharge profiles of full and half cells based on graphite anodes and PTCDI cathodes. **d** Charge/discharge profiles of different cycles and lighted signs lit by full batteries. **e** Cycling performance of a full cell at 80 mA g^{-1}. **f** Comparison of the properties and performances of the 1 M KFSI in EC/DCC and EC/DEC electrolytes.

■ ACKNOWLEDGMENTS

J. Peng and X. Yi contributed equally to this work. This work was financially supported by the National Natural Science Foundation of China (Nos. U20A20247, 51922038, and 52101252).

■ CONFLICT OF INTEREST

The authors declare no conflict of interest.

■ AUTHOR CONTRIBUTIONS

Authors Jun Peng, Xianhui Yi, and Jiang Zhou discussed the study and analyzed the data. Authors Jun Peng, Xianhui Yi, Ling Fan, and Bingan Lu wrote the article. The author, Bingan Lu, supervised the whole work. All authors had approved the final version.

■ REFERENCES

1. W. Zhang, Y. Liu, Z. Guo, *Sci. Adv.*, 2019, 5, eaav7412
2. J. Li, Y. Hu, H. Xie, J. Peng, L. Fan, J. Zhou, B. Lu, *Angew. Chem. Int. Ed.*, 2022, 61, e202208291
3. B. Xiao, H. Zhang, Z. Sun, M. Li, Y. Fan, H. Lin, H. Liu, B. Jiang, Y. Shen, M.-S. Wang, M. Li, Q. Zhang, *J. Energy Chem.*, 2023, 76, 547
4. M. Ma, S. Zhang, L. Wang, Y. Yao, R. Shao, L. Shen, L. Yu, J. Dai, Y. Jiang, X. Cheng, Y. Wu, X. Wu, X. Yao, Q. Zhang, Y. Yu, *Adv. Mater.*, 2021, 33, 2106232
5. L. Fan, R. Ma, Q. Zhang, X. Jia, B. Lu, *Angew. Chem. Int. Ed.*, 2019, 58, 10500
6. Y. Hu, L. Fan, A. M. Rao, W. Yu, C. Zhuoma, Y. Feng, Z. Qin, J. Zhou, B. Lu, *Natl. Sci. Rev.*, 2022, 9, nwac134
7. L. A. Schkeryantz, J. Zheng, W. D. McCulloch, L. Qin, S. Zhang, C. E. Moore, Y. Wu, *Chem. Mater.*, 2020, 32, 10423
8. Z. Yu, P. E. Rudnicki, Z. Zhang, Z. Huang, H. Celik, S. T. Oyakhire, Y. Chen, X. Kong, S. C. Kim, X. Xiao, H. Wang, Y. Zheng, G. A. Kamat, M. S. Kim, S. F. Bent, J. Qin, Y. Cui, Z. Bao, *Nat. Energy*, 2022, 7, 94
9. S. Liu, J. Mao, Q. Zhang, Z. Wang, W. K. Pang, L. Zhang, A. Du, V. Sencadas, W. Zhang, Z. Guo, *Angew. Chem. Int. Ed.*, 2020, 59, 3638
10. J. Ming, Z. Cao, W. Wahyudi, M. Li, P. Kumar, Y. Wu, J.-Y. Hwang, M. N. Hedhili, L. Cavallo, Y.-K. Sun, L.-J. Li, *ACS Energy Lett.*, 2018, 3, 335
11. E. P. Kamphaus, S. Angarita-Gomez, X. Qin, M. Shao, M. Engelhard, K. T. Mueller, V. Murugesan, P. B. Balbuena, *ACS Appl. Mater. Interfaces*, 2019, 11, 31467
12. H. Wang, D. Zhai, F. Kang, *Energy Environ. Sci.*, 2020, 13, 4583
13. M. Gauthier, T. J. Carney, A. Grimaud, L. Giordano, N. Pour, H.-H. Chang, D. P. Fenning, S. F. Lux, O. Paschos, C. Bauer, F. Maglia, S. Lupart, P. Lamp, Y. Shao-Horn, *J. Phys. Chem. Lett.*, 2015, 6, 4653
14. Y. Lei, D. Han, J. Dong, L. Qin, X. Li, D. Zhai, B. Li, Y. Wu, F. Kang, *Energy Stor. Mater.*, 2020, 24, 319
15. Y. Li, Q. Zhang, Y. Yuan, H. Liu, C. Yang, Z. Lin, J. Lu, *Adv. Energy Mater.*, 2020, 10, 2000717

DOI: 10.54227/elab.20220014

16. K. Shi, L. Chen, Z. Wan, J. Biao, G. Zhong, X. Li, L. Yang, J. Ma, W. Lv, F. Ren, H. wang, Y. Yang, F. Kang, Y.-B. He, *Sci. Bull.*, 2022, 67, 946
17. Z. Chen, B. Wang, Y. Li, F. Bai, Y. Zhou, C. Li, T. Li, *ACS Appl. Mater. Interfaces*, 2022, 14, 28014
18. X. Zheng, L. Huang, W. Luo, H. Wang, Y. Dai, X. Liu, Z. Wang, H. Zheng, Y. Huang, *ACS Energy Lett.*, 2021, 6, 2054
19. Z. Hou, R. Zhou, Y. Yao, Z. Min, Z. Lu, Y. Zhu, J.-M. Tarascon, B. Zhang, *Angew Chem. Int. Ed.*, 2022, 61, e202214796
20. B. Gangaja, S. Nair, D. Santhanagopalan, *Sustain. Energy Fuels*, 2019, 3, 2490
21. S. Liu, X. Ji, N. Piao, J. Chen, N. Eidson, J. Xu, P. Wang, L. Chen, J. Zhang, T. Deng, S. Hou, T. Jin, H. Wan, J. Li, J. Tu, C. Wang, *Angew. Chem. Int. Ed.*, 2021, 60, 3661
22. L. Droguet, G. M. Hobold, M. F. Lagadec, R. Guo, C. Lethien, M. Hallot, O. Fontaine, J.-M. Tarascon, B. M. Gallant, A. Grimaud, *ACS Energy Lett.*, 2021, 6, 2575
23. X. Fan, X. Ji, F. Han, J. Yue, J. Chen, L. Chen, T. Deng, J. Jiang, C. Wang, *Sci. Adv.*, 2018, 4, eaau9245
24. K. Subramanian, G. V. Alexander, K. Karthik, S. Patra, M. S. Indu, O. V. Sreejith, R. Viswanathan, J. Narayanasamy, R. Murugan, *J. Energy Stor.*, 2021, 33, 102157
25. C. Fang, J. Li, M. Zhang, Y. Zhang, F. Yang, J. Z. Lee, M.-H. Lee, J. Alvarado, M. A. Schroeder, Y. Yang, B. Lu, N. Williams, M. Ceja, L. Yang, M. Cai, J. Gu, K. Xu, X. Wang, Y. S. Meng, *Nature*, 2019, 572, 511
26. H. Kitaura, E. Hosono, H. Zhou, *Energy Environ. Sci*, 2021, 14, 4474
27. A. Ramasubramanian, V. Yurkiv, T. Foroozan, M. Ragone, R. Shahbazian-Yassar, F. Mashayek, *J. Phys. Chem. C*, 2019, 123, 10237
28. J. Pan, Q. Zhang, X. Xiao, Y.-T. Cheng, Y. Qi, *ACS Appl. Mater. Interfaces*, 2016, 8, 5687
29. S. Yuan, S. Weng, F. Wang, X. Dong, Y. Wang, Z. Wang, C. Shen, J. L. Bao, X. Wang, Y. Xia, *Nano Energy*, 2021, 83, 105847
30. C. Stetson, M. Schnabel, Z. Li, S. P. Harvey, C.-S. Jiang, A. Norman, S. C. DeCaluwe, M. Al-Jassim, A. Burrell, *ACS Energy Lett.*, 2020, 5, 3657
31. Y. Rangom, R. R. Gaddam, T. T. Duignan, X. S. Zhao, *ACS Appl. Mater. Interfaces*, 2019, 11, 34796
32. J. Zhu, P. Li, X. Chen, D. Legut, Y. Fan, R. Zhang, Y. Lu, X. Cheng, Q. Zhang, *Energy Stor. Mater.*, 2019, 16, 426
33. F. Yuan, J. Hu, Y. Lei, R. Zhao, C. Gao, H. Wang, B. Li, F. Kang, D. Zhai, *ACS Nano*, 2022, 16, 12511
34. K. Yan, H.-W. Lee, T. Gao, G. Zheng, H. Yao, H. Wang, Z. Lu, Y. Zhou, Z. Liang, Z. Liu, S. Chu, Y. Cui, *Nano Lett.*, 2014, 14, 6016
35. J. Fondard, E. Irisarri, C. Courrèges, M. R. Palacin, A. Ponrouch, R. Dedryvère, *J. Electrochem. Soc.*, 2020, 167, 070526
36. L. Ma, C. Fu, L. Li, K. S. Mayilvahanan, T. Watkins, B. R. Perdue, K. R. Zavadil, B. A. Helms, *Nano Lett.*, 2019, 19, 1387
37. Y. Zhao, M. Amirmaleki, Q. Sun, C. Zhao, A. Codirenzi, L. V. Goncharova, C. Wang, K. Adair, X. Li, X. Yang, F. Zhao, R. Li, T. Filleter, M. Cai, X. Sun, *Matter*, 2019, 1, 1215
38. Y. Zhou, M. Su, X. Yu, Y. Zhang, J.-G. Wang, X. Ren, R. Cao, W. Xu, D. R. Baer, Y. Du, O. Borodin, Y. Wang, X.-L. Wang, K. Xu, Z. Xu, C. Wang, Z. Zhu, *Nat. Nanotechnol.*, 2020, 15, 224
39. Z. Wang, C. Sun, Y. Shi, F. Qi, Q. Wei, X. Li, Z. Sun, B. An, F. Li, *J. Power Sources*, 2019, 439, 227073
40. D. Kang, S. Sardar, R. Zhang, H. Noam, J. Chen, L. Ma, W. Liang, C. Shi, J. P. Lemmon, *Energy Stor. Mater.*, 2020, 27, 69
41. X.-Q. Zhang, X.-B. Cheng, X. Chen, C. Yan, Q. Zhang, *Adv. Funct. Mater.*, 2017, 27, 1605989
42. X. Ren, Y. Zhang, M. H. Engelhard, Q. Li, J.-G. Zhang, W. Xu, *ACS Energy Lett.*, 2018, 3, 14
43. Y. Liu, X. Tao, Y. Wang, C. Jiang, C. Ma, O. Sheng, G. Lu, X. Wen, *Science*, 2022, 375, 739
44. Z. Lin, X. Guo, R. Zhang, M. Tang, P. Ding, Z. Zhang, L. Wu, Y. Wang, S. Zhao, Q. Zhang, H. Yu, *Nano Energy*, 2022, 98, 107330
45. Q. Liu, A. M. Rao, X. Han, B. Lu, *Adv. Sci.*, 2021, 8, 2003639
46. D. Hulicova-Jurcakova, M. Kodama, S. Shiraishi, H. Hatori, Z. H. Zhu, G. Q. Lu, *Adv. Funct. Mater.*, 2009, 19, 1800
47. Z. Gu, G. Li, N. Hussain, B. Tian, Y. Shi, *Appl. Surface Sci.*, 2022, 592, 153323
48. A. Ponrouch, R. Dedryvère, D. Monti, A. E. Demet, J. M. Ateba Mba, L. Croguennec, C. Masquelier, P. Johansson, M. R. Palacín, *Energy Environ. Sci.*, 2013, 6, 2361
49. Y. Gao, X. Du, Z. Hou, X. Shen, Y.-W. Mai, J.-M. Tarascon, B. Zhang, *Joule*, 2021, 5, 1860
50. X.-Q. Zhang, X. Chen, X.-B. Cheng, B.-Q. Li, X. Shen, C. Yan, J.-Q. Huang, Q. Zhang, *Angew. Chem. Int. Ed.*, 2018, 57, 5301
51. D. Lu, X. Lei, S. Weng, R. Li, J. Li, L. Lv, H. Zhang, Y. Huang, J. Zhang, S. Zhang, L. Fan, X. Wang, L. Chen, G. Cui, D. Su, X. Fan, *Energy Environ. Sci.*, 2022, 15, 3331